Journal of Engineering Research 13 (2025) 2053–2065

Contents lists available at ScienceDirect

Journal of Engineering Research

journal homepage: www.journals.elsevier.com/journal-of-engineering-research

Thermos-aerodynamic performance and heat transfer analysis in a rectangular channel using various angle groove geometry

Samson A. Aasa [a,*], Gazi I. Mahmood [a,b]

[a] Department of Mechanical and Aeronautical Engineering, University of Pretoria, South Africa
[b] Department of Mechanical Engineering, Prince Mohammed Bin Fahd University, Al Khobar, Saudi Arabia

ARTICLE INFO

Keywords:
Groove Pitch
Pressure penalties
Friction factors
Nusselt number
Performance index and Flow visualisation

ABSTRACT

The effects of heat transfer and friction factors are critical portions of an endwall passive technique to achieve an optimum level of thermal index. In this study, three groove endwalls arranged at 45° to the axial flow direction with only one side of endwalls is wholly covered with angled grooves roughened surface while the other sides are kept smooth. The three grooved endwalls use in this study have relative pitch roughness, P/δ, print diameter, D_p, and inclined at an angle to flow direction, (i.e., P/δ = 13, D_p=2; P/δ = 9, D_p= 2; P/δ = 6.5, D_p=4; and α = 45 °). The groove endwalls are then used to measure the channel pressure drop and enhanced heat transfer from the surface of the plate. IR Camera is also used to study the flow full field behavioural effect at various groove arrangements and Reynolds numbers ($600 \geq Re \leq 11000$). The outcomes reveal the effect of friction factors, Nusselt number, and performance index at the Reynolds number *Re* and 5 mm channel. The experiments presented figures for f_G, f_G/f_0, *Nu*, Nu/Nu_0, and thermal performance, $[Nu_G/Nu_0/(f_G/f_0)^{1/3}]$. From the results of the investigation, the groove roughened surfaces enhance the heat transfer, generate moderate pressure penalties, and improve it performance index. In addition, the flow structural full-field patterns confirm and further demonstrate how uniform distributions of the flow in the downstream section of the groove are represented in each of the endwalls. The Nusselt number comparison of the upstream and downstream sections of the test section show the flow full-field behaviours at the downstream sections are uniformly distributed compared to upstream sections. This turbulence distribution improve as the Reynolds number within the channels changes and relative pitch roughness significantly influences the mixing rate within the channel.

Introduction

Internal cooling schemes have been discovered as one of the best ways to eliminate or reduce the impact of pressure penalties on control surfaces heat exchanger devices. The enhancement techniques have therefore been identified to offer high performance characteristics, moderate pressure penalties, and improved surface enhancement, to mention a few. These endless possibilities and effectiveness in heat exchanger devices are due to little or no aerodynamic penalties, nonthermal bond contact, and small air inlet characteristic requirements. The application of such techniques in heat exchanger devices tends toward increasing enhancement of turbulence level and secondary flow field mixing in some form of articulate fluid vortices. These are known to give a high level of turbulence transport to flow field for optimal system performance. Thus, they are not only propagating secondary advection but also 3D turbulence flow through velocity gradient and increasing shear for approximately level flow mixing characteristics. Achieving this, however, requires a detailed understanding of flow augmentation of surface heat transfer and flow structure characteristics that give optimal thermal protection at minimal coolant [1–5].

Previous studies on internal passive cooling techniques have been used by many researchers to analyse the effects of groove/rib surface combinations [2]. Saha and Acharya [2] carried out flow augmentation system in a rectangular channel using various combinations of grooves and rib arrangements. From the results, cooling passages in an airfoil enhanced the heat transfer performance. This, in its sense, is extracted from a high-pressure compressor, which is achieved in excess of 20 % total air. From the study, this could only be accomplished through an in-depth understanding of the existing strategies, especially those with moderate pressure penalties. This was also confirmed by other studies using different combinations; however, high pressure penalties affect

* Corresponding author.
E-mail address: aasa.aasa@tuks.co.za (S.A. Aasa).

https://doi.org/10.1016/j.jer.2024.09.003
Received 23 April 2024; Received in revised form 1 September 2024; Accepted 2 September 2024
Available online 5 September 2024

the system performance characteristics [3–5]. The combined passive techniques such as dimples-ribs, dimple-pin fins, and grooves-ribs to enhance the system performance for optimal thermal protection and moderate pressure penalties had been studied [6,7]. Liu et al., [6] carried out turbulent flow in a square cylindrical groove duct, the study carried out optimal heat enhancement augmentation. In this study, different circular bottom grooves were utilised, it was revealed that the pressure drop of circular groove geometry was not as high as that of the triangular groove, and the systems improved the thermal efficiency. The results were compared with existing results and with flow details in groove surface predicted.

In addition, infrared thermography was used to study heat transfer in rectangular grooves. The results show that the Nusselt number ratio is in the range of 1.52 – 1.75 as established by [8]. Eimsa-Ard and Promvonge [9] investigated turbulence forced convection using the periodic transverse groove. Four turbulence models were used to conduct the finite-volume method: renormalised-category k–ω, Shear Stress-Transport, SST k–ω, normal–k–ω, and standard k–ω. The analysis was carried out for Re 6000–18000 and aspect ratio 0.5–1.75. The groove heat transfer relative to the smooth channel employed in the study were 1.58 and 1.33. The thermal efficiency of the groove aspect ratio is 0.75. Consequently, the transverse groove in a rectangular duct with recirculation could increase the rate of heat transfer. The cross-section of the grooves was used to examine the characteristics of the heat transfer and friction factor according to [10]. But this occurred more in the tube than those of circular, rectangular, trapezoidal, and triangular geometries. In comparison to circular and trapezoidal grooves, one (l) groove with smooth bottom curves and triangular grooves had the strongest effects on the Nusselt number but also produced high-pressure penalties. This was further corroborated by [7,11] on rectangular ducts. Ramadhan et al., [7] numerically supported these results using a two-dimensional duct with four grooves of similar configurations. Optimal performance protection was observed for low groove depth. However, no major emphasis has been placed on the characteristics of groove pitch, depth, or orientation techniques. These parametric behavioural experiments are limited to open literature. According to Saha and Acharya [2], small ($p/\delta = 10$) and large ($p/\delta = 15$) pitch-angled grooves were conducted in a simulated rectangular internal cooling channel, with the grooves arranged at 45° to the flow direction and using a transient liquid crystal for Re = 13000–55000. Their results showed that the large groove performance was slightly lower than the small-pitch groove performance, reflected in heat transfer and pressure drop penalties. Furthermore, numerical analysis of the transverse V-shaped groove on the flow and wall mass transfer [12] was performed using four separate groove roughened walls and the Reynolds number protected from to 103–105. The influences of the Reynolds number, groove thickness, and groove pitch on the transfer of the wall mass and near-wall flow were studied. The denser and shallower the grooves, the higher the mass transfer rate. Also, increasing the Reynolds number weakened the enhancement effect. The V-triangular groove in the triangular base channel was also studied by [13], which doubled the triangular depth and heated the channel symmetrically to achieve greater efficiency than the smooth channel. The results revealed a completely formed flow after just four typical grooves, which was maintained until the end of the groove wall. At the vortex of the groove face, a thin thermal boundary layer adjacent to the groove face was observed with a non-uniform heat flux distribution. Eventually, it was found that the windward Nusselt number was double the leeward number. The parameters for the local heat transfer on the rough groove endwall were further studied numerically [14,15], the result showed a similar result however, the parametric internal flow fields characteristics were not discussed. This limited the output to the common knowledge.

In addition, using a numerical comparative study of novel groove geometries [16], the authors determined the optimal increase in heat transfer. The results showed minimal pressure loss a vantage point for applications, hence, orthodox cylindrical grooves were better suited to heat improvements. Flow reattachment was also noted to have been refined with minimal system separation. The immense velocity of the nearest wall allows the device to provide improved heat transfer. The outcome and thermal performance of the dimple structure are of particular interest compared to those of grooves. Adachi and Hasegawa [17] numerically analyzed the transition region of the recurrent grooved channel for oscillation indices m, which ranged from 1 to 6 and were groove periodicity numbers for continuous flow repetitions in the channels. Adachi et al., [18], investigated experimentally the characteristic pressure decrease in periodically arranged grooves. Oscillatory resilience growth due to the periodic flow of fluid in the canal resulted in a significant increase in fluid heat transfer and pressure drop penalties. In this case, the pressure drop characteristics were found to increase at the critical point of the groove end, and the Reynolds number increased where two-and three-dimensional oscillation occurs. Flow visualization was used to investigate the three-dimensional flow of the grooved channel. The critical Reynolds number at the pivotal stage of steady-state oscillatory flow separation was calculated using numerical simulations. The groove pitch doubled the oscillatory flow of the fluid in the tube. The numerical evidence is reviewed and is found to be consistent with the experimental results. Some significant constraints need to be discussed in the methodological development of an internal thermal enhancement strategy. Consistent research in all affected areas should be expanded to satisfy these criteria. The use of passive techniques in all areas of heating and cooling, such as airfoil surfaces, aerodynamics, electronic appliances, fuel cells, solar panels, heat transfer, and thermal considerations, must be understood. The studies emphasized the need for a research trend to focus more on internal thermal protection schemes, especially as the material components necessary for coolant temperature are not feasible. Thus, designers, manufacturers, and researchers must develop an internal cooling system to provide an improved thermal performance index for the operating system [19].

Few studies on the characteristics of such applications have been devoted to the physical properties and interactions of their parameters. This certainly has significant effect on the enhancement and performance characteristics. However, heat enhancement and flow full-field interaction that provide internal details of the performance process in these passive techniques, particularly in grooved plate applications, have been limited. This entails detailed augmentation process, which must be understood to provide robust progression and an advantageous internal surface design. In this study, various pitches in an inclined groove surface in the flow direction were used to examine flow augmentations. The aerodynamic and flow benefits of these types of applications are yet to be fully reconnoitred in improving the flow performance of heat-exchanger devices [1]. Therefore, using a rectangular channel, the flow structure augmentation and heat transfer over a one-sided grooved endwall are investigated for flow enhancement. Studies have shown that this could be the driving solution for the depth of heat fluctuation in heat exchanger devices, especially when an extended system performance is desirable [2–5]. From this review, very little information exists on experiments that consider the use of groove modification techniques for internal passages to increase heat transfer despite their potential. In addition, the experimental flow distribution accounts are minimal especially those with IR camera which present advanced details with flow internal structures that provides valuable insight and information to understand the output of thermos-aerodynamics performance.

Methodology

Experimental setup and descriptions

Test Section and instrumentation

The experimental setup for the open-circuit low-speed wind channel

built for this study is shown in Fig. 1. The wind channel consists of an air straightener, reducer, smoothly organized inlet channel, test section, outlet channel, plenum chamber, pipe sections, and blower box. The collection was installed with a low-speed blower fan at the end of the pipe. The inlet channel is approximately 2.0 m long, and the test segment is 0.5 m long, as is the outlet section of the channel. The plenum chamber is a rectangular chamber where the flow settles before it moves to two pipe Sections (2- and 4-inch pipes) for the high- and low-Reynolds-number experiments. For the channel, a standard rectangular cross-section of 203 mm with an adjustable height from the lower outlet to the inlet of the plenum chamber was used. The material for the segment of the plate and wind channel was made of a polycarbonate acrylic plate. The removable end wall of the test section was 203 mm in width, with wall thicknesses of 6 mm and 12 mm for the heat transfer and pressure drop experiments, respectively. In compliance with the International Standard Organisation, (ISO), a pipe section was built based on ISO-1567 [20] for the assembly of orifice plates and flange measurements. While a 2-inch (57 mm) pipe diameter was used for the low Reynolds number measurement of Re $<$ 2000, a wide 4-inch (100 mm) pipe diameter was used for the higher Reynolds number, Re $>$ 2000. The mass flow rate and Reynolds number in the rectangular channel were controlled and regulated by variable speed drive, (VSD). When the pressure drops and thermocouple positions were tapped through the end wall, the pressure drop rubber tube was locked in, and the same was performed for the thermocouples. Fig. 1(b) and (c) show the arrangement of the heat transfer plate, heater position, insulation layers, and thermocouples on the heated endwall.

Pressure taps with a thickness of 12 mm made on a 203 mm wide endwall were used for pressure measurement. Similarly, for the measurement of heat transfer, a wall with a width of 6 mm and a width of 203 mm was used for heater transfer experiments, insulation, and thermocouples for the measurement of surface temperature. The standard copper tape heater was smoothly welded to each other at intervals of 1 mm on the smooth side of the plate used to cover the entire 203 mm width of the test section plate, and the thermocouple was then tapped to allow surface temperature measurement. The entire area of the test section was protected by the heater. Pressure taps were attached to the multiport scanner values, from which the differential pressure transducer was used to collect data from plastic pressure using LabView software. Pressures on the orifice plate were collected by separate differential pressure transducers using the National Instrument™ Data Acquisition Setup System. Thermocouple heat-transfer measurements were performed using a thermocouple. The surface temperature in the test section, which is the insulation temperature for conduction losses during the experiment, was acquired by directly connecting the thermocouple to the multiport National Instrument™ Data Acquisition Outlet.

The differential pressure transducer signal data were digitized at a sampling rate of 100 Hz for 2 s and then time-averaged to output the data recorded in the LabView™ data log, which was then converted into a pressure unit using calibration measurements. The same was done for the thermocouples; in this case, the output was an average of 2 KHz for

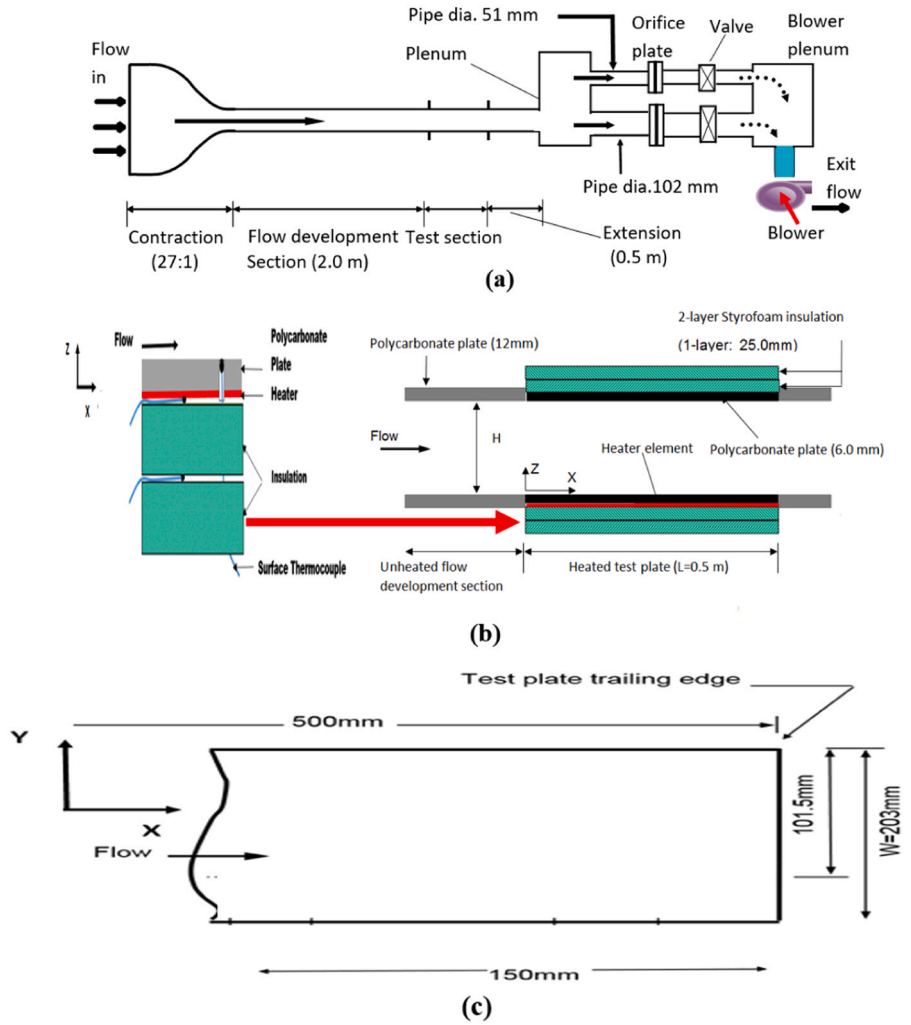

Fig. 1. (a) Schematic Diagram of test facility (b) Heater arrangement along the test Section (c) Endwall Heat transfer plate.

2 s and recorded in the LabView™ program. It was then obtained from appropriate calibration measurements. Furthermore, using the direct current, (DC), power supply, the required power is supplied to the system from the applied voltage and current adjusted to meet the demand from the mass flow rate until a minimum difference of 10 °C is obtained between the bulk temperature airflow and wall temperature. The details of the mean bulk temperature of the flow are given in Eq. (1). It estimates the temperature along the heated wall of the test section based on the energy balance between the inlet and streamwise locations (x = 0 – L). Where $T_{a,in}$ is the inlet temperature, which is taken as ambient air temperature of the unheated air; $\sum Q_{cx}$is summation of the convective heat losses; Qcx, is the convective power. The conduction losses in this study were less than 5 % of the total heated power. Therefore, the total convective heat flux was assumed to be constant. Using each thermocouple location along the endwall, the local Nusselt number Nu_x is estimated by the expression in Eq. (2). Aasa et al., [21]

$$T_{m,x} = T_{a,x} + \frac{\sum Q_{c,x}}{m_a . C_p} \tag{1}$$

$$Nu_x = \frac{Q_c \bullet D_h}{[(L \bullet W) \bullet (T_{w,x} - T_{m,x}) \bullet K_a]} \tag{2}$$

Where, Q_c, is the average convective heat flux in the stream L, W are the length and width of the heated plate, and $T_{w,x}$ is the wall temperature at each of the thermocouple locations; $T_{m,x}$ Mix-mean temperature of the thermocouple.

Infrared (IR) camera and thermal imaging

The flow structure interactions of the experiments were performed using a Flir™ IR camera. Flir™ S35sc captured the thermal image of the heated groove of the endwall. The picture obtained from the device offers a continuous distribution of the heat transfer coefficient or Nusselt number along the groove surface. The infrared camera was calibrated from 18 to 60 °C and operated with a lens of 48 °and a frame rate of 60 Hz. For the optical access of the camera, two circular cut-out sections in a 203 mm thick smooth wall (unheated wall) opposite the heated groove surface were used. A zinc-selenide (Zn-Se) window or an acrylic-plastic window was used for the cut-out pieces. The cut-out window located on the smooth wall opposite to the grooved endwall was used as a saw through for the IR camera full-field data acquisition. In the range of 5–100 μm, the antireflection coated Zn-Se window was transparent to the infrared wavelength. The Zinc-Selenide window has a diameter of 50 mm and is situated 40 mm upstream and 450 mm downstream of the inlet of the test portion (see picture for details of the frame window). Spray-tinted black is the target region of the heated groove surface for thermal imaging to decrease reflections and increase emissivity on the surface (= 0.95). There were 13 and 11 thermocouples in the upstream and downstream window sections, respectively. The method proposed by Sargent et al. [22] was used to calibrate the image based on an in-situ calibration technique. The thermocouples were embedded in the wall, with the tips placed only on the surface. As the small geometries of both the groove and thermocouple tip were comparable, no thermocouples were mounted in the area. The infrared camera was positioned horizontally at the center of the cut-out window to capture an image of the groove wall. It is noteworthy that a blank acrylic-plastic window was used to cover one of the windows when the Zn-Se window was used in one place, while the other took the image. The pitch width of 10.5 cm by 10.5 cm is filled by a camera with a pixel size of 0.4 mm×0.5 mm at each endwall position. With the in-situ procedures in [23,24], the calibration of the camera image is carried out against the temperature of the groove wall thermocouples located in the image region. Fig. 2(a) shows the arrangement of the IR camera against the test section. The sample calibration curve generated from IR measurements is shown in Fig. 2(b). In addition, as described by [25], a second-order polynomial regression

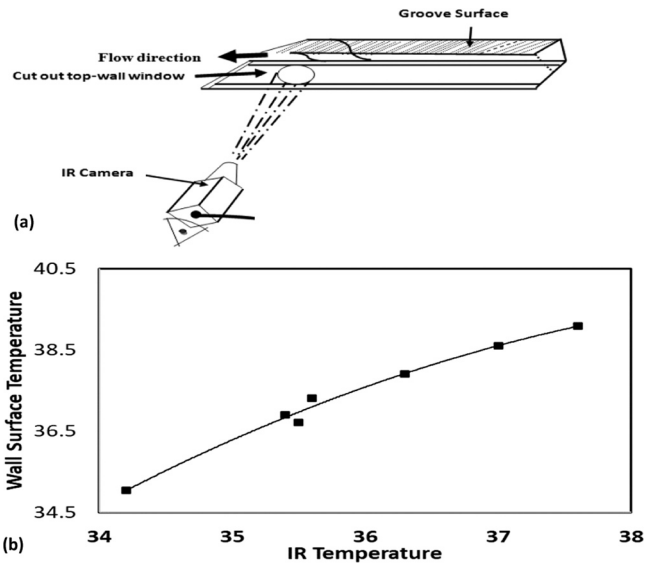

Fig. 2. (a) Thermal Infrared Camera set up (b) Sample of Insitu Calibration curve for IR camera imaging.

data fit was applied. The known pixel size and location of the thermocouple were then used to determine the spatial position of the image pixel. Twenty image samples were captured on the spot and averaged at each of the window positions under steady thermal conditions of the groove wall.

Groove endwall geometry

Three grooved endwalls were examined in this analysis. The grooves are semi-circular and are periodically machined at an angle of 45 °all over the width of the plate relative to the axial direction of flow (plate length) in the Computer Numeric Control, (CNC), unit. Commercial-quality acrylic-plastic grooved plates with a thickness of 12 mm and a thickness of 6 mm were used for heat transfer measurements. The grooves were fabricated in an array that varied in geometry relative to the array pitch, groove width, and groove print diameter from plate to plate. Table1.1 indicates the geometry of the grooves used in the three test plates. The grooves were organized at a 45-degree angle to the flow direction, as shown in Fig. 3(a-c). Fig. 3(a) shows the first case: P/δ = 9, r_G = 1 mm, and D_p = 2 mm. Fig. 3(b) shows the second case: P/δ= 13, r_G = 1 mm, and D_p = 2 mm. The third case is shown in Fig. 3(c): P/δ = 6.5, r_G = 2 mm, and D_p = 4 mm. The X-coordinates represent the flow direction, whereas the Y-coordinates represent the distance along a width of 203 mm. Measurements were performed at three channel heights of 5 mm.

Uncertainty analysis

After boot-welding the thermocouples, they were calibrated. The accuracy of the differential pressure transducers was 2 Pa and a 0.1 °C accuracy was observed in the thermocouples. Calibration bias errors were accounted for in the measurements. Analysis of the total and

Table 1.1
Details of groove geometry and operating range.

Groove #	D_p- Groove diameter (mm)	P-Groove Pitch (mm)	δ (mm)	H (mm)	$δ/D_p$	P/δ	δ/H
1	2	9	1	5	0.5	9	0.2
2	2	13	1	5	0.5	13	0.2
3	4	13	2	5	0.5	6.5	0.2

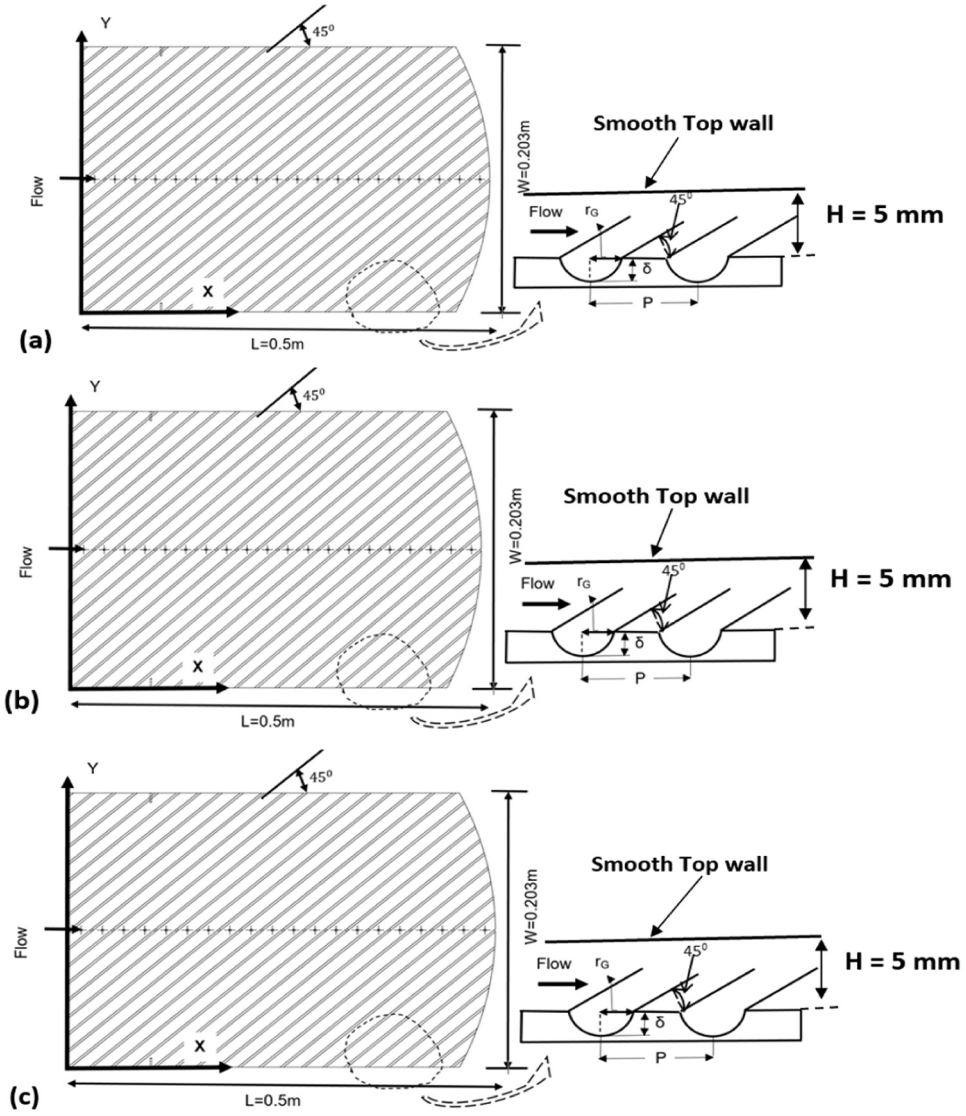

Fig. 3. Groove plate details, geometric for; (a) P/δ = 9 (b) P/δ = 13, (c) P/δ = 6.5.

precision uncertainties in the calibration, measurement, and estimates was performed [22–26]. According to the experimental outcome estimation process, the mass flow rate uncertainties were ≤ 2 %, the pressure drop uncertainties were ≤ 2.5 Pa. the calculated friction factor uncertainties were ≤ 3.5 %. The maximum heat flux uncertainty is ≤ 3.5 %, and the maximum temperature uncertainty is ± 0.5 °C. The Nusselt number uncertainty was calculated as ≤ 5 %. The maximum uncertainty in the thermal performance was 5.5 %. The variations in the uncertainty were due to the fabrication tolerances, Re changes, axial conduction, and heat flux variations.

Results and discussions

The tests were carried out for both the pressure drop and heat transfer experiments after all the necessary procedures for the experiment were observed. The data for each experiment were obtained at the steady state of the flow when the fluctuations of pressure and temperature readings were within +2 Pa and 0.1 °C, respectively; these were observed to occur within 10 – 15 min. The experiment was conducted for a Reynolds number that varied between 600 –15000 (600 ≥ Re ≤ 15000). The inlet test section air properties for the flow were estimated at the ambient condition of the inlet for air pressure and temperature changes below 1 kPa and 20 $^{°C}$, respectively, from the inlet to the exit of the test section. Using a suitable heat flux dependent on *Re*, a constant heat flux boundary condition was applied to both the smooth and grooved endwalls. The normalized friction factors and Nusselt number were calculated using the baseline results measured using a smooth channel section. It should be noted that the walls were adiabatic (no heating) for all pressure-drop experiments. The flow structure experiments conducted using an infrared camera also provided details of the flow heat transfer, and the results were compared with the average local thermocouples and Nusselt number results at various *Re* values.

Pressure drop and friction factor

For the pressure drop results, smooth and grooved endwall channel results were obtained. In this investigation, only the smooth route data for the grooved endwall were provided. Next, the grooved wall data were normalised along the grooved endwall test section x/L's streamwise direction.

Fig. 4 illustrates this for groove plates with P/δ values of 9, 13, and 6.5, and a channel height of 5 mm. The normalised pressure decrease, ΔP*, for Reynolds numbers 600 ≥ Re ≤ 15000 at various groove pitches is shown in these data. Equation (3) is used to calculate the normalised pressure drop, or ΔP*, from the recorded wall static pressure; the reference pressures, px and p0, are collected at a distance of about 30 cm

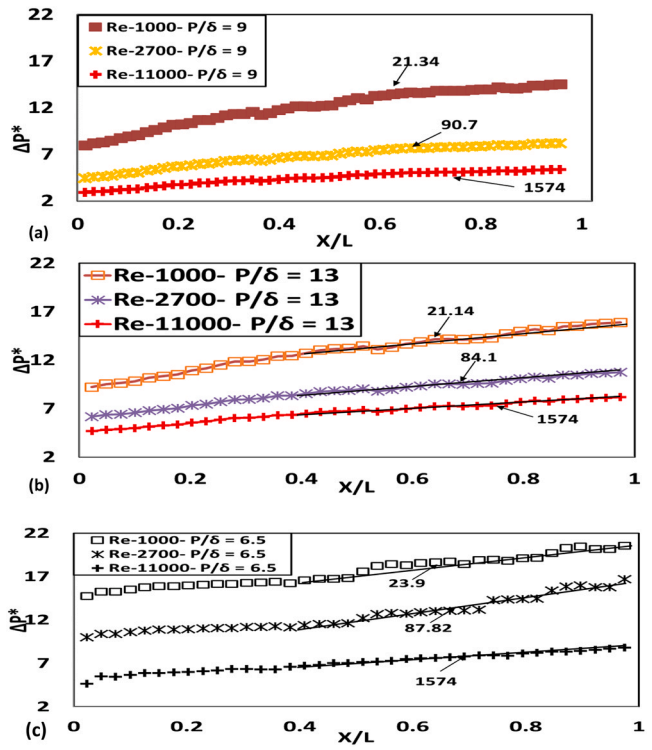

Fig. 4. Normalized pressure drop for groove plates at Channel Height H = 5 mm with (a) P/∂ = 9, (b) P/∂ = 13, and (c) P/∂ = 6.5.

upstream of the test section. Fig. 4 displays the test section inlet, denoted by x/L = 0. The normalized pressure drops, ΔP*, distribution along the channel, and for each of the groove plates at different pitches decrease as the Reynolds number increases, and vice versa. The distributions also indicate the effect of groove pitches. The pressure drops from P/δ= 6.5 is noticed to are the highest, followed by P/δ = 9, and finally P/δ = 13. This shows that as the flow moves through the successive grooves with some spark of flow along the channel wave, the distribution of the pressure drop ($p_x - p_o$) is affected. A square fit line was observed as a straight line in the linear regression analysis. The square line of fit through the data point along x/L for each of the groove plates indicates an almost straight constant line of fit. R^2 correlation coefficient values of 0.97 are obtainable for the line fits. This shows that the flow was hydrodynamically fully developed in the groove channel [21,27].

$$\Delta P^* = \frac{p_x - p_0}{0.5 * \rho V^2} \quad (3)$$

Fig. 5 shows the experimental friction factors and Nusselt numbers compared with the analytical correlations. The experimental friction factor baseline was compared to the analytical correlations of Shah and London and Karma Nikuradse [28,29]. The results revealed a variation of less than 5 % (Fig. 5(a)). Similarly, Fig. 5(b) presents the experimental Nusselt number compared with the analytical correlation of the Dittus Boelter [30]. The results show a maximum variation of less than 5 % for all Reynolds numbers and experiments carried out.

The friction factor for the experiment is presented in Fig. 6 using Eq. (4). This was estimated from the channel pressure drop distribution Δp/Δx. The pressure drop, Δp/Δx, along the channel was obtained from the line of fit for each Reynolds number. The friction factors versus Reynolds number for groove plates with relative pitch roughness, P/δ, of 9, 13, and 6.5, and at a channel height of 5 mm are presented. The friction factors for P/δ = 9, 13, and 6.5 at a channel height of 5 mm and 600≥Re≤15000 are reported in the plot. The groove friction factor f_G decreased as Re increased in all grooved plates. A sharp and sudden decline was observed in the first section of the flow from the laminar to transition regimes. Thereafter, in the turbulent region, a gradual decrease was observed with a small variation in the friction factor f_G as the Reynolds number increased. Generally, the friction factor decreased

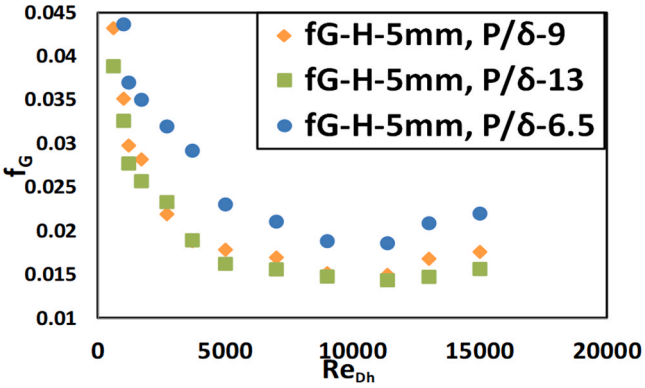

Fig. 6. Groove Average Friction factor, f_G, against Re for P/δ = 9, P/δ = 13 and P/δ = 6.5, at H = 5 mm.

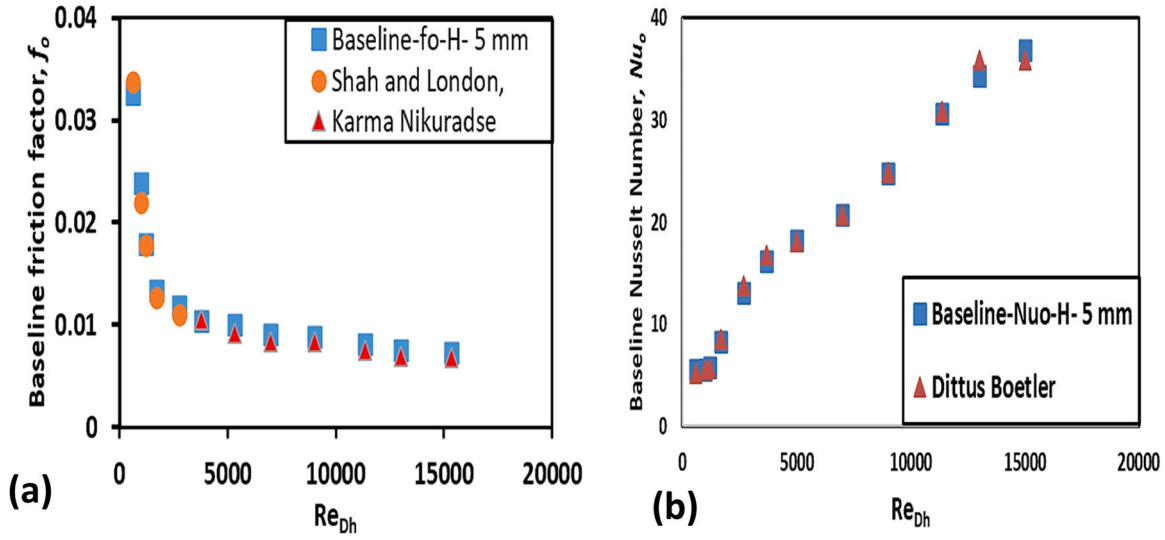

Fig. 5. Baseline Friction factor and Nusselt Number, at H = 5 mm (a) Friction factor, f_o, (b) Nusselt Number, Nu_o.

as the relative pitch roughness increased. This clearly shows that the relative pitch roughness, P/δ, 6.5 has higher friction factors compared to the relative pitch roughness, P/δ, 9, which has higher friction factors compared to the relative pitch roughness, P/δ, 13. For the laminar regime with Re≤ 2000, viscous friction is prominent and more drag friction is observed in the transition regime Re > 2000 as a result of high turbulence flow in this regime Aasa et al., [31].

$$f = \frac{\left(\frac{\Delta p}{\Delta x}\right) \bullet \left(\frac{D_h}{4}\right)}{0.5 * \rho * V^2} \tag{4}$$

In addition, the periodic effect of grooves on the friction factor performance at various pitches of the grooved plates and at a channel height is sufficiently evident that the pitch influences the friction factor. The f_G varies between 0.035–0.045 for Re ≥ 2000, 0.023–0.035 for Re≤5000 and 0.018 – 0.022 for Re ≤15000. A negligible variation in friction factors is observed for Re ≥ 7000, which is a fully turbulent regime. The friction factor ratios for the grooved plates at various pitches are presented in Fig. 7. The friction factor ratios for groove plates with relative pitch roughness, P/δ, of 9, 13, and 6.5, at a channel height, H, of 5 mm. From the data presented in Fig. 7, an increase in friction factor ratios, f_G/f_0, is observed from the laminar to turbulence regime for Re≤2000, then exponentially as Re reaches the transition regime Re<5000, and then drops slightly from 5000≥Re≤7000 before it starts to gradually increase again as soon as it reaches the fully turbulent regime 7000≥Re≤15000 in each of the groove pitches. All the groove pitches have multiple effects of a minimum friction factor of 1.3 % and 2.7 %, which occur at Reynolds numbers of 600 and 15000, respectively. The highest groove effect was observed with a relative pitch roughness of P/δ = 6.5, followed by P/δ = 9, and P/δ = 13. This shows that the grooves influence the flow augmentation.

Nusselt number

This section discusses the Nusselt number distributions as represented in the text section, the average local Nu_x, and the average Nusselt number ratios, Nu_{xavg}/Nu_{0avg}, for the endwall heated boundary. From Eqs. (1) and (2), the groove channel Nusselt number Nu_x and smooth channel Nusselt number Nu_0 were estimated using the average constant heat flux across the endwall and the recorded surface wall temperature.

Fig. 8 shows the data for the grooved plate with a relative pitch roughness P/δ of 9 at a channel height of 5 mm and 600 ≥ Re ≤ 15000. In this figure, the local Nusselt number distribution along x/L in the test section begins approximately 2 m from the inlet of the test facility. The Nusselt number distributions decreased downstream of the test section as the thermal flow developed until it reached the steady state at x/L = 0.4, where a minute change in the local Nusselt number was observed along the channel at various Re and groove plates. The negligible

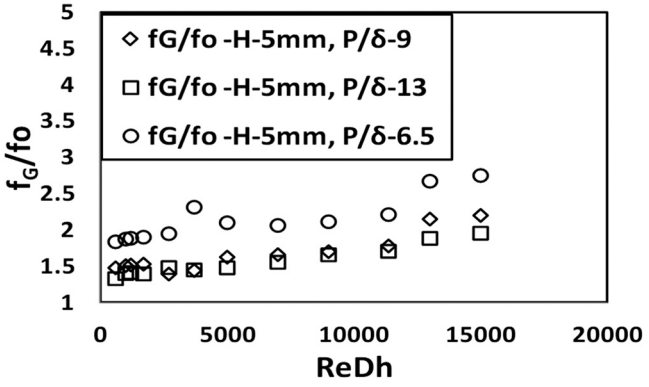

Fig. 7. Friction factor ratio, f_G/f_o, against Reynolds Number for P/δ = 9; 13; 6.5 at H – 5 mm.

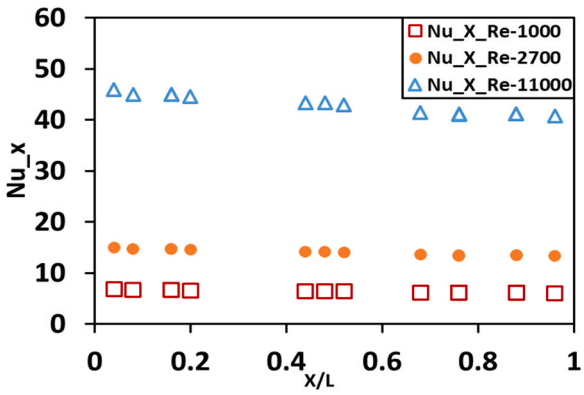

Fig. 8. Local Nusselt Number against channel length, x/L, for P/δ = 9; H – 5 mm for 1000≥Re≤11000.

variation in the Nusselt number as the thermal flow develops is due to a reduction in the turbulent flow in the channel.

The average Nusselt number, Nu_{avg}, is presented in Fig. 9(a) for various pitch-to-depth ratios (P/δ = 9, 13, 6.5), and 600≥Re≤15000, is obtained from the average local Nusselt number in the flow-developed region of the channel. Fig. 9(a) shows that Nu_{avg} increases as the Reynolds number changes across the flow regimes. However, the groove plate P/δ = 6.5 with a large pitch (13 mm pitch) has the highest Nu_{avg}. This may be related to the groove size at a depth of 2 mm. Next, the groove plate P/δ = 9 (9 mm pitch) with a 1 mm depth, and the groove plate P/δ = 13 (13 mm pitch) with a 1 mm depth had the lowest Nusselt number at various Re values. The data distributions indicate that the periodic nature of the flow analysis of the groove affects the flow distribution and thermal development. The higher the grooves, the more turbulation of the flow, and therefore, the better the thermal distribution. This finding was confirmed by Acharya and Saha [2]. The depth of the groove has a higher thermal effect than its pitch. This is observed in grooved plates with P/δ = 6.5 and P/δ = 13. Even though they have the same groove pitches, the variation in the depth of the grooves, which determines how close the pitches make a big difference in $Nu_{avg,}$ is observed in all regimes of flow (laminar transition and turbulence regimes) and channel heights. As a result, at a channel height of 5 mm and 600≥Re≤15000 groove plates with a pitch-to-depth ratio P/δ = 6.5, $Nu_{avg,}$ which varies between 9 and 88; the pitch-to-depth ratio P/δ = 9 presents $Nu_{avg,}$ which varies between 7 and 73; and the pitch-to-depth ratio P/δ = 13 presents $Nu_{avg,}$ which varies between 6 and 68. Thus, the periodic groove pitch influences the thermal development for flow augmentation in the channel.

The ratios of the groove channel average Nusselt number to the smooth channel average Nusselt number, Nu_{avg}/ Nu_{0avg}, are presented in Fig. 9(b). In general, the plot shows that the distribution of Nu_{avg}/ Nu_{0avg}, increases from the laminar to the turbulent regime for 600≥Re≤15000 and at different groove plates and channel heights. This figure shows a relative pitch roughness P/δ of 9. 13, and 6.5 at 5 mm, and 600≥Re≤15000. The groove surfaces influence the heat transfer with all plates, given a factor greater than one (1). According to this graph, the groove plate P/δ = 6.5 has the highest effect with Nu_{avg}/ Nu_{0avg} ranging from 1.30 – 2.45 %; followed by the groove plate P/Î = 9 with the smallest pitch with Nu_{avg}/ Nu_{0avg} ranging from 1.18 – 1.8 % and groove plate P/δ = 13 with Nu_{avg}/ Nu_{0avg} ranging from 1.1 % to 1.75 %. The Nu_{avg}/ Nu_{0avg} shows a sharp increase in distributions at the onset of the flow for lower Re < 2000; this drops for Re < 7000, after which it rises steadily throughout the turbulence regime of the experiments for Re≤15000.

The performance index of the flow was estimated using the ratio Nu_{avg}/Nu_{0avg} to $(f_G/f_0)^{1/3}$ [29]. The heat transfer enhancements show that the groove plates enhance the performance index of fluid flow. Generally, the performance index in all groove plates was higher than

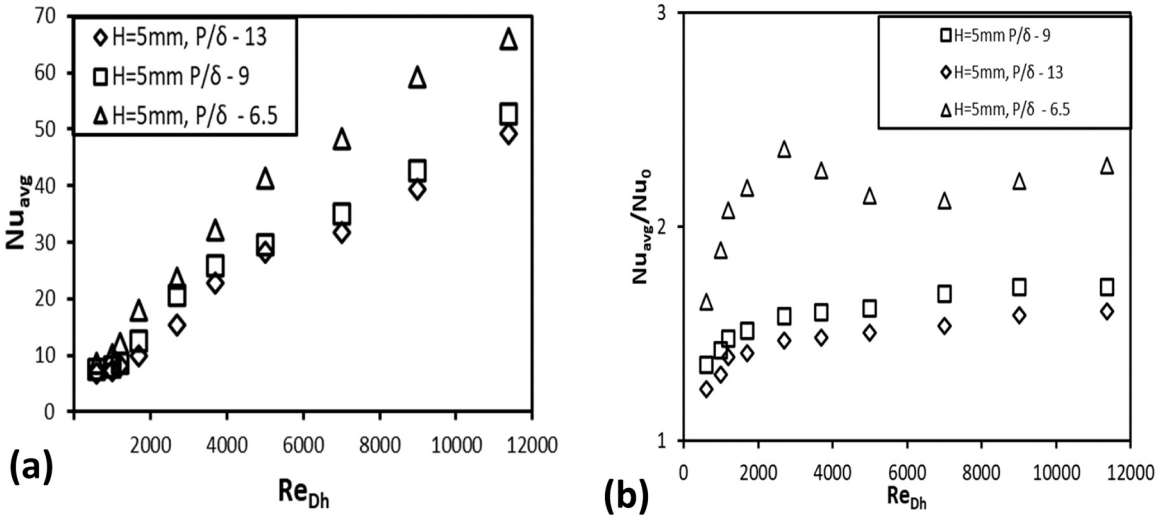

Fig. 9. (a) Average Nusselt Number against Reynolds Number for (b) Average Nusselt Number ratio, Nu_{avg}/Nu_o, against Reynolds Number.

one (1.0). This implies that the performance factors of the groove plate heat transfer and moderate friction factors were improved. The thermal performance data presented in Fig. 10 show a steady increase for Re < 3000 for the laminar regime and then drops slightly for the transition regime range, and it thereafter picks up a little before it reaches a stable state with negligible variation for the turbulence regime 7000 ≥ Re ≤ 15000. The denser and shallower the grooves, the higher the mass wall transfer rate; however, an increase in the Reynolds number weakens the enhancement effects. Grooves offer excellent performance compared to other proven literature-based geometries. This is because it blends both the characteristics of the dimples and the groove structures noted for mild pressure (pressure drops) penalties for heat-transfer enhancement.

Flow full-field Interaction

To adequately determine the flow distribution of the heat transfer in this experiment, an IR camera was used to visualize the flow of the system. Following a step-by-step acquisition technique as expressed in the design section, the data are processed for upstream and downstream flow visualization, which is presented in Figs. 11 – 13 for the groove plate with relative pitch roughness P/δ of 9, 13, at 6.5, and a channel height of 5 mm.

From the flow visualizations (Figs. 11 – 13), the relative pitch roughness (P/δ) effects were well pronounced. The upstream data presented in the figures show how the flow floods the surface of the groove with little or no impact, which is typical for smooth channels. However, a uniform distribution was observed in all upstream sections.

In the downstream sections, the data presented for groove plates with a relative pitch roughness, P/δ, of 6.5 shows the highest effect of all the grooves. This results in a high turbulence effect at Re ≥ 5000 and a smoother distribution as the flow reaches a high Re ≥ 7000.

However, the flow distribution for the plate with a P/δ of 9 had a moderate distribution compared to the flow at P/δ = 13 with a less definite uniform distribution. These are observed at a low Re and groove relative pitch roughness, P/δ, of 6.5, and 9, respectively. It is worth noting that the flow improves with a moderate irregular flow distribution as Re increases. Even at P/δ = 13, the flow distribution was uniform at Re ≥ 7000 and higher Re.

Therefore, it is noteworthy that the impact of the groove in this section (upstream section) of the flow is far less significant than that in the downstream section of the test facility with uniformly mixed flow and high turbulence performance index.

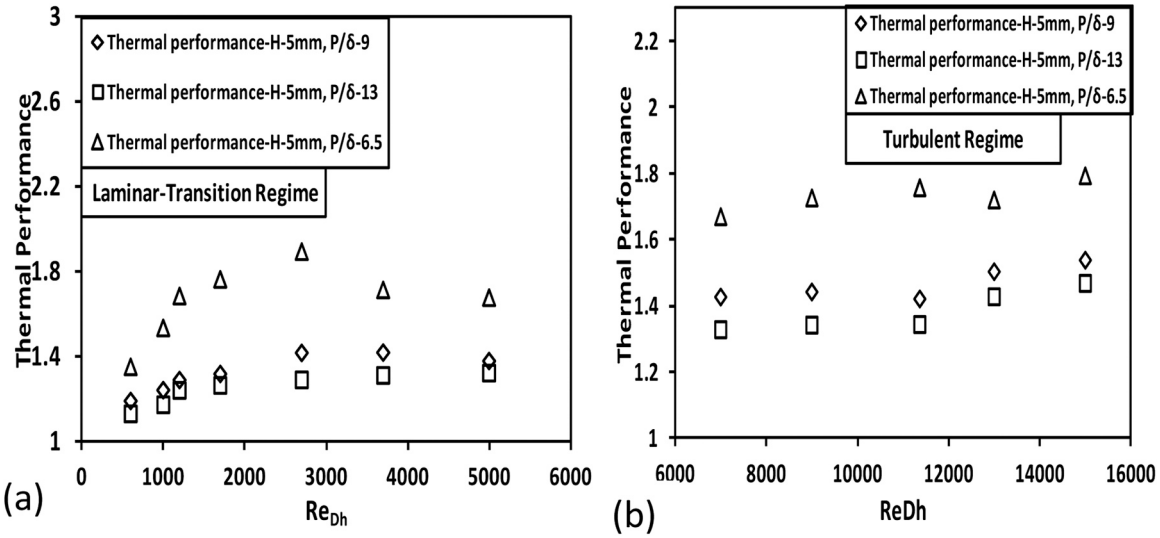

Fig. 10. Thermal Performance Index against Reynolds numbers for grooved plates P/δ = 9; P/δ= 13 and P/δ = 6.5 at channel Height, H – 5 mm (a) Laminar-Transition regimes(b) Turbulent regime.

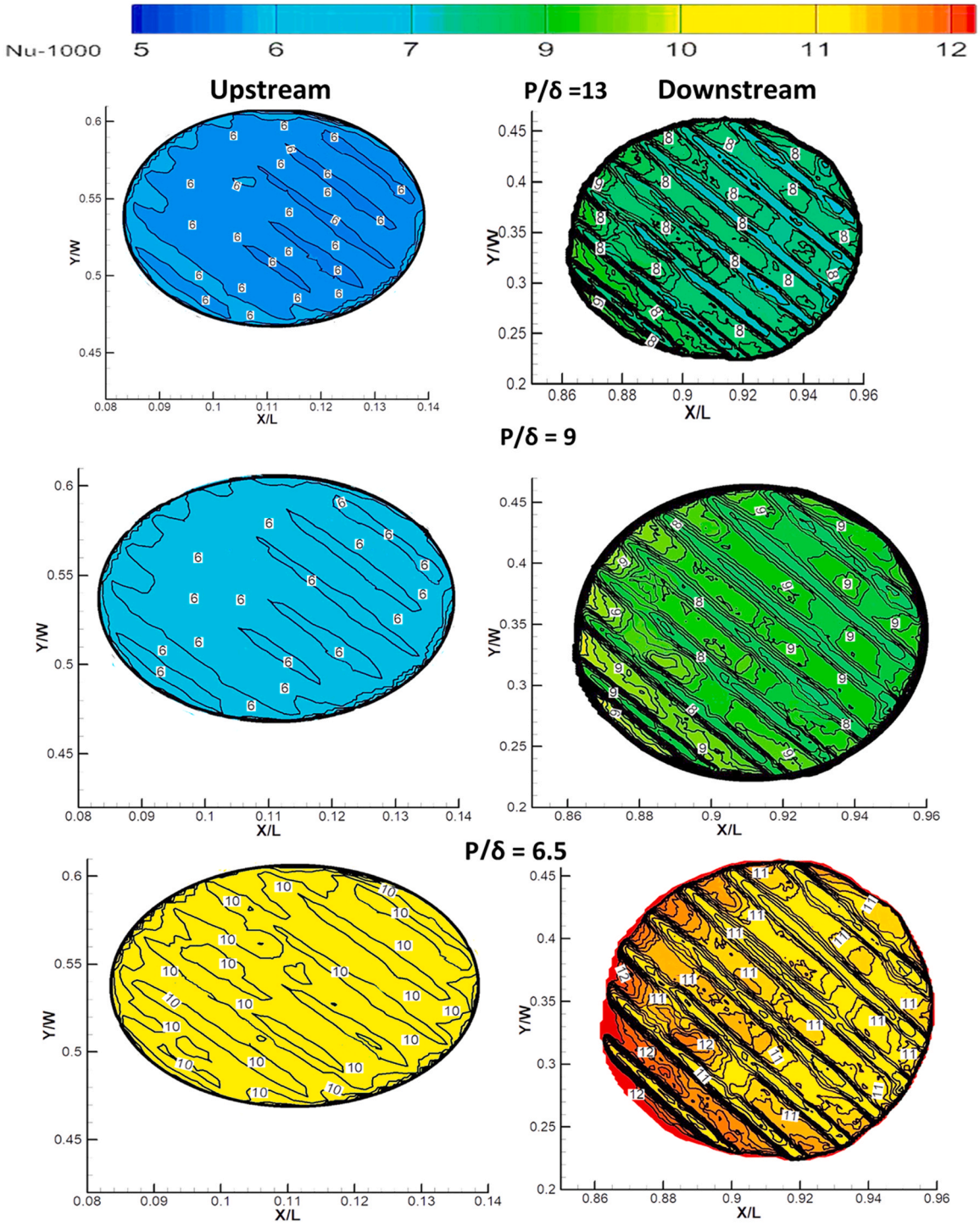

Fig. 11. IR Flow full-field images for upstream and downstream at H = 5 mm and 1000 Re.

Conclusions

A study was carried out to investigate how convective heat is enhanced in rectangular channels. Heat improvements employing different grooved surfaces were carried out in this study to give a more thorough grasp of its thermal performance and behavioural characteristics. The study utilised groove models with relative pitch roughness (P/δ) values of 9, 13, and 6.5. (Pitch, P = 9 mm; depth, δ = 1 mm; Pitch, P = 13 mm; depth, δ = 1 mm; Pitch, P = 13 mm; and δ = 2 mm). For this experiment, data were gathered from every grooved plate with a 5 mm channel height. The data validations give context for the data integrity by utilising the heat transfer coefficient and pressure drop correlations that are currently in place. The information provided is thought to be helpful in figuring out how different parameters—such as air temperature, friction factors, Nusselt number, pressure drop, and IR visualisation images of heat transfer coefficients at the upstream and downstream sections behave and perform in a semi-circular groove that is prescribed on a regular basis. This study presents the behaviour of these factors in a rectangular channel. The groove angle was set at 45 °to the flow stream direction, and it covered a surface area of 203 mm × 500 mm in the test section. The channel employs only a one-sided groove surface, and the other surfaces remain smooth. Data were acquired only from the

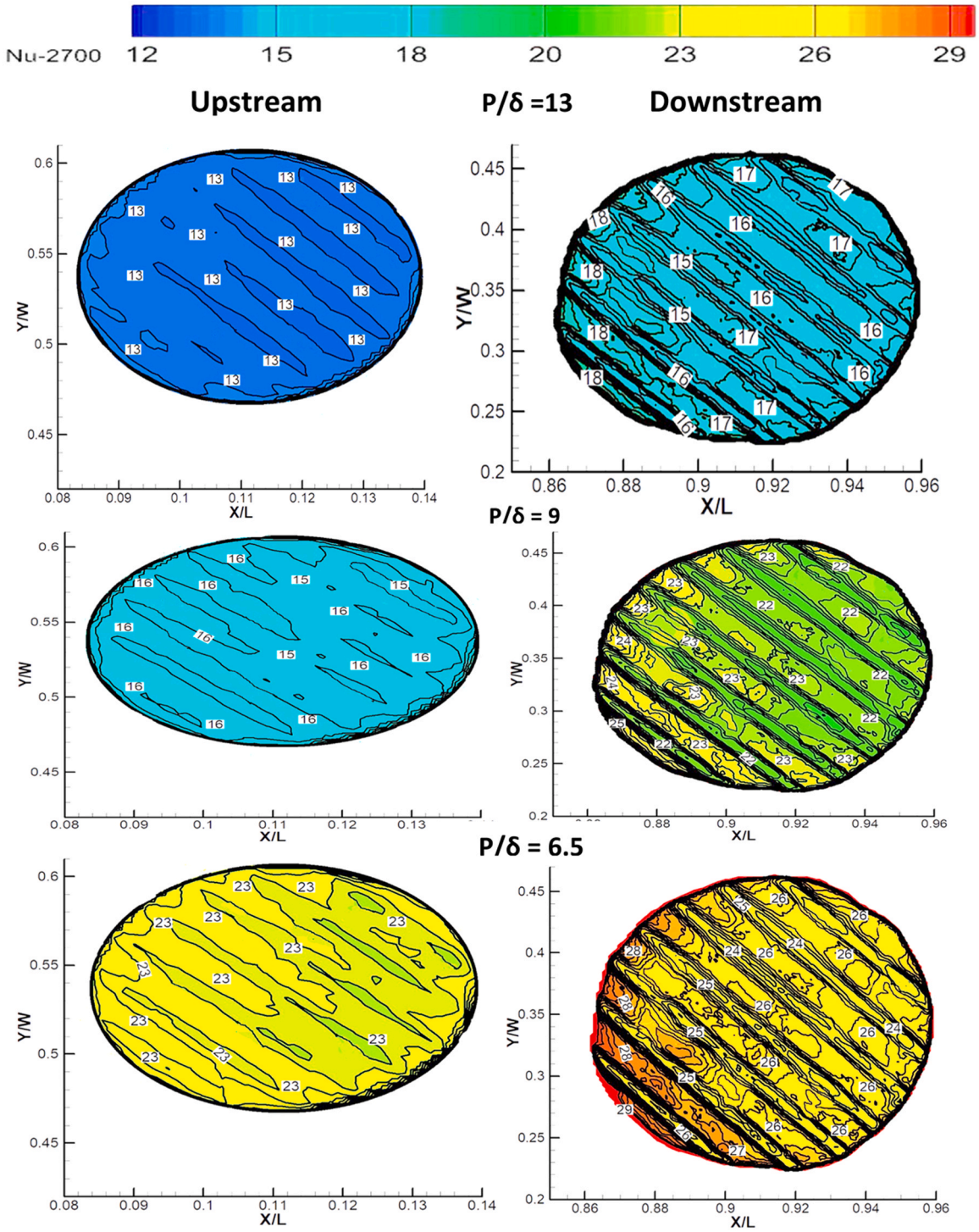

Fig. 12. IR Flow full-field images for upstream and downstream at H = 5 mm and 2700 Re.

grooved wall. A constant heat flux plate was attached to the outer surface of the groove wall, and the Reynolds numbers, as stipulated in this study, were set between 600 and 15000. Therefore, the experiment imitates the application of a typical passive enhancement in fuel cells, internal turbine vane cooling, and photovoltaic cells.

The experiment's measurements and results led to the following deductions:

When the tests were run for the same Reynolds number, the pressure distribution along the mainstream of the test section obtained for the baseline was uniform and modest with permitted uncertainty. The baseline's average friction factors and average Nusselt number closely matched the correlations that had previously been used in the investigation. Because of the angled groove that turbulates the fluid flows and affects the temperature and pressure drops during the experiment, it was found that the flow field in the grooved instances was largely uniform with occasional spikes. Consequently, the fluid flow characteristics, friction factor, pressure drop, temperature, and Nusselt number were all improved by the grooved end-wall alteration. The test section's gradient was obtained by measuring the pressure decrease along its mainline, from which the friction factors were computed. Every tested groove

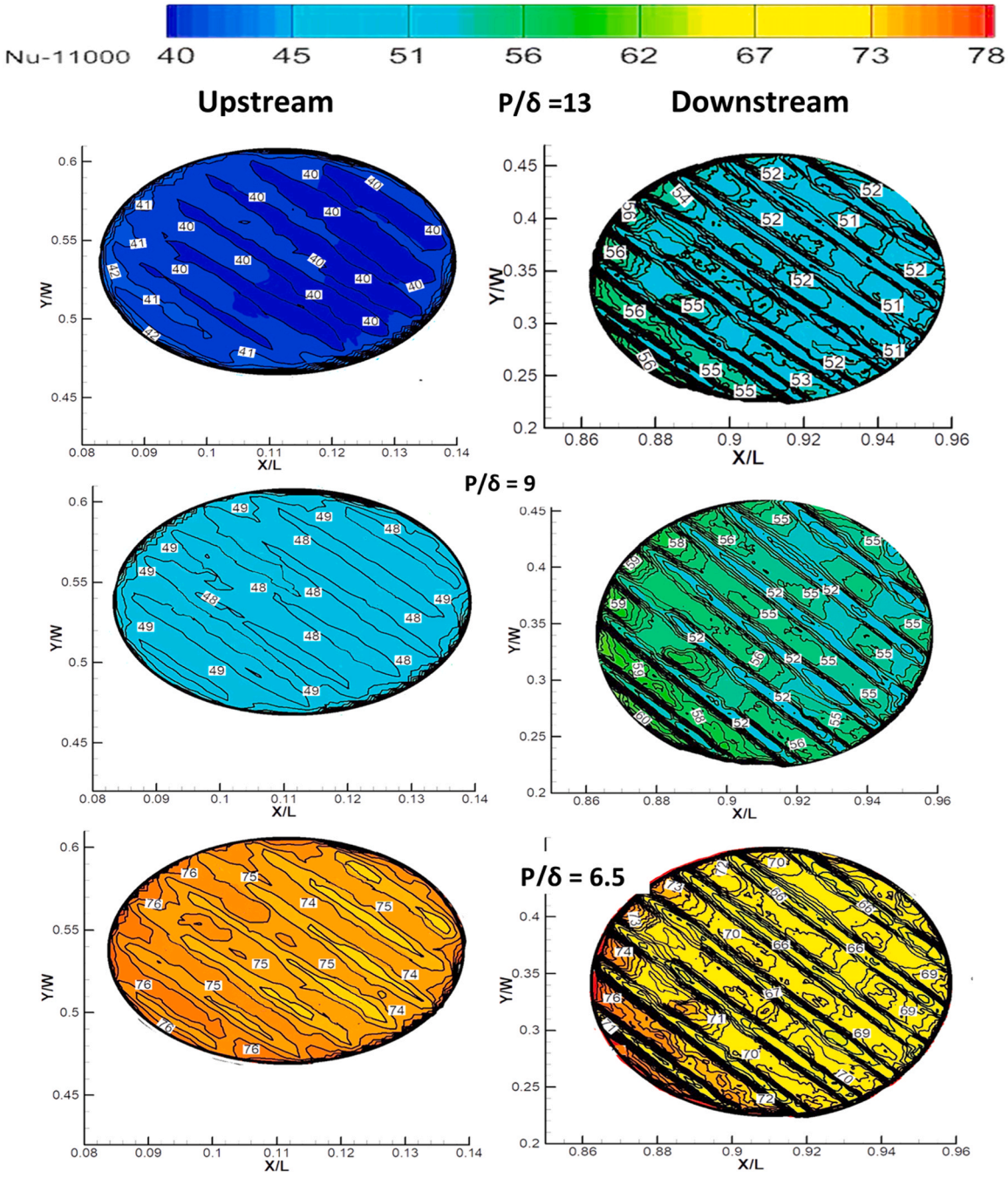

Fig. 13. IR Flow full-field images for upstream and downstream at H = 5 mm and 11000 Re.

offered precise behavioural patterns and representations. Consequently, the fluid flow characteristics, friction factor, pressure drop, temperature, and Nusselt number were all improved by the grooved end-wall alteration. The test section's gradient was obtained by measuring the pressure decrease along its mainline, from which the friction factors were computed. Every tested groove offered precise behavioural patterns and representations. To this end, the grooves improved the friction factor with the optimum performance obtained from the groove plate, P/δ = 6.5. A maximum friction factor ratio of 2.7 occurs atRe = 15000 and a channel height, H, of 5 mm.

The raw temperature data collected from the majority of the channel test section was used to calculate the Nusselt number and heat transfer coefficient for this investigation. The data was then corrected using the calibration curve equation. Every groove offered a precise depiction and pattern of behaviour for examination. This shows that the grooves increase the Nusselt number and groove plate with a relative pitch roughness, P/δ, of 6.5, which best influences the fluid. An average Nusselt number ratio of 2.98 occurred atRe = 15000 and a channel height of 5 mm. The Nusselt number ratios for the other groove plates, P/δ, of 9 and 13 follow the same pattern. Therefore, all plates are judged to be effective at a Reynolds number. The thermal performance index for the angled groove plates showed that the grooves improved system performance. The model with a relative pitch roughness, P/δ, of 6.5 (Pitch, P, of 13 mm and depth, δ, of 2 mm) had the best performance of all the grooved plates.

The Nu_{IR} heat transfer visualization data, both upstream and downstream of the test section, show the flow-characteristic distributions in these regions. The Nusselt number flow structure images

upstream and downstream of the test section showed a uniform distribution across the surfaces of the grooves. The results show that the groove plates P/δ = 9 and P/δ = 13 have similar performance index results for all channel heights considered. Even though the pitches on these plates varied, the output results did not vary significantly. The effect of pitch on system performance is not as important as the depth of the groove. This makes the groove case with a relative pitch roughness, P/δ, of 6.5 best performed in all the cases under study. A similar observation was recorded when large- and small-pitch grooves were considered in Saha and Acharya (2014).

In general, these are the main conclusions of this study:

- Re_{Dh} is a dependent parameter of the friction factor f_G and the friction factor ratio f_G/f_0 in the channel. An increase in the Reynolds number increased the friction factor.
- The friction factor ratio, f_G/f_0, rises until the 2700 – 5000 *Re* range, when the pressure drops slightly and then rises throughout the turbulence region $7000 \geq Re \leq 15000$.
- The heat transfer, Nu_{avg}/Nu_o, for the 5 mm channel (aspect ratio 0.025) was the highest, and all Nusselt numbers increased with an increase in Re_{Dh} at a given groove relative pitch roughness.
- The angled grooves have an effect on the flow full-field visualisations, and it is further verified that the fluid field flows are specifically impacted by the separations, the orientation of the grooves, and the impingement rate.
- The lower boundary layer thickness and longer fluid flow separation time on the groove surfaces produced the greatest results, according to the visualisation distribution.

The findings are helpful for enhancing the thermal performance and geometry of heat exchangers in cooling or heating channel application domains, such as generator jackets, bearing jackets, fuel cells, electronic components, photovoltaic cells, and turbine blades.

The authors also recommend that five hole probes and/or particle velocimetry be used to conduct more thorough internal flow full field experiments.

Nomenclature

(A_c, D_h)channel cross-sectional area, hydraulic diameter
(c_p, k_a)(specific heat, thermal conductivity) of air
*f*friction factor in screen channel
(H, L, W) (height, length, width) of test section
$m_a$mass flow rate of air
NuNusselt number
(P_x, P_0, P*) Pressure: local wall-static, reference, normalized on wall
(Q_c, $Q_{c,x}$)(total convective power, local convective power) on surface
ReReynolds number, $\left(\frac{m_a D_h}{A_c \mu_a}\right)$
($T_{a,in}$, $T_{m,x}$, $T_{w,x}$) Temperature: inlet air, local bulk-mean of air, on wall at distance X
Umean flow velocity, $\left(\frac{m_a}{A_c \rho_a}\right)$
(X, Y, Z)
P/δ
δ/D_hCartesian coordinate system
Relative pitch roughness
Relative depth roughness
Greek Symbols
Δdifference between two quantities
(μ_a, ρ_a)(dynamic-viscosity, density) of air
Subscripts and Superscripts
avgaverage property
xlocal property on the wall along X
0reference or smooth channel property

CRediT authorship contribution statement

Gazi I. Mahmood: Writing – review & editing, Visualization, Validation, Supervision, Funding acquisition, Data curation, Conceptualization. **Samson Abiodun Aasa:** Writing – review & editing, Writing – original draft, Visualization, Project administration, Methodology, Investigation, Formal analysis, Conceptualization.

Declaration of Competing Interest

This paper titled “Heat Transfer and Thermos-Aerodynamic Performance Analysis Using Angle Groove Geometry in A Rectangular Channel” is a product of empirical research.

The study’s main contribution is to provide information on passive heat enhancement system related to heat exchanger devices’ performances. We are very confident that the results of the study are essential information for the academics, policymakers, and practitioners for developing policy frameworks.

We ascertain that this manuscript has not been submitted elsewhere for publication. The author and/or co-authors also do not have financial or non-financial competing interest. We would be grateful if this request for publication were granted.

References

[1] P.W. Bearman, J.K. Harvey, Golf ball aerodynamics, Aeronaut. Q (1976) 112–122.
[2] K. Saha, S. Acharya, Heat transfer enhancement using angled grooves as turbulence promoters, J. Turbomach. 136 (8) (2014).
[3] P.M. Ligrani, G.I. Mahmood, D.L. Nelson, J.L. Harrison, C.M. Clayton, Flow structure and local nusselt number variations in a channel with dimples and protrusions on opposite walls, Int. J. Heat. Mass Transf. Vol. 44 (No. 23) (2001).
[4] M.K. Chyu, Y. Yu, H. Ding, J.P. Downs, F.O. Soechting, Concavity Enhanced Heat Transfer in an Internal Cooling Passage, American Society of Mechanical Engineers, 1997. Paper 97-GT-437.
[5] N. Zhao, L. Guo, C. Qi, T. Chen, X. Cui, Experimental study on thermo-hydraulic performance of nanofluids in CPU heat sink with rectangular grooves and cylindrical bugles based on exergy efficiency, Energy Convers. Manag. 181 (2019) 235–246.
[6] J. Liu, G. Xie, T.W. Simon, Turbulent flow and heat transfer enhancement in rectangular channels with novel cylindrical grooves, Int. J. Heat. Mass Transf. 81 (2015) (2015) 563–577.
[7] A.A. Ramadhan, Y.T. Al, A.J. Anii, Shareef, Groove geometry effects on turbulent heat transfer and fluid flow, Heat. Mass Transf. 49 (2013) 185–195.
[8] S. Lorenz, D. Mukomilow, W. Leiner, Distribution of the heat transfer coefficient in a channel with periodic transverse grooves, Exp. Therm. Fluid Sci. 11 (1995) 234–242.
[9] S. Eiamsa-ard, P. Promvonge, Numerical study on heat transfer of turbulent channel flow over periodic grooves, Int. Commun. Heat. Mass Transf. 35 (2008) 844–852.
[10] K. Bilen, M. Cetin, H. Gul, T. Balta, The investigation of groove geometry effect on heat transfer for internally grooved duct, Appl. Therm. Eng. 29 (2009) 753–761.
[11] S. Eiamsa-ard, P. Promvonge, Thermal characteristics of turbulent rib-grooved channel flows, Int. Commun. Heat. Mass Transf. 36 (2009) 705–711.
[12] Y. Zhang, D. Che, Numerical simulation of turbulent flow and wall mass transfer in a rectangular channel roughened by V-Shaped grooves, Numer. Heat. Transf., Part A 66 (2015) 551–581.
[13] A.R. Wirtz, F. Huang, M. Greiner, Correlation of fully developed heat transfer and pressure drop in a symmetric grooved channel, J. Heat. Transf. 121 (1999) 236–239.
[14] P.S. Lee, C.J. Teo, Heat Transfer Enhancement in Microchannels Incorporating Slanted Grooves, ASME Paper No. 08-MNHT-52374 (2008).
[15] E.H. Ridouane, A. Campo, Heat transfer enhancement of air flowing across grooved channels: joint effects of channel height and groove depth, J. Heat. Transf. 130 (2008) 1–7.
[16] Baghernezhad, N. and Abouali, O., (2008), Numerical Investigation of Single Phase Heat Transfer Enhancement in a Microchannel with Grooved Surfaces, ASME Paper No. 08-ICNMM-62262.
[17] T. Adachi, S. Hasegawa, Transition of the flow in a symmetric channel with periodically expanded grooves, Chem. Eng. Sci. 61 (8) (2006) 2721–2729.
[18] T. Adachi, Y. Tashiro, H. Arima, Y. Ikwgami, Pressure drop and characteristic of flow in a symmetric channel with periodically expanded grooves, Chem. Eng. Sci. 64 (3) (2009) 593–597.
[19] C. Wang, Z.L. Liu, G.M. Zhang, M. Zhang, Experimental investigations of flat plate heat pipes with interlaced narrow grooves or channels as capillary structure, Exp. Therm. Fluid Sci. 48 (2013) 222–229.
[20] International Standard Organization, ISO 5167-1980(E), Measurement of Fluid Flow by Means of Orifice Plates, Nozzles and Venture Tubes Inserted in Circular Cross-Section Conduits Running Full, 1980-07-15.

[21] S.A. Aasa, A.S. Shote, S.O. Giwa, M. Sharifpur, Friction factor effect and heat transfer enhancement in combined dimple geometry arrange in different angle to flow direction, Elsevier J. Fuel Commun. (2021), https://doi.org/10.1016/j.jfueco.2021.100043.
[22] S.R. Sargent, C.R. Hedlund, P.M. Ligrani, An infrared thermography imaging system for convective heat transfer measurement in complex flows, Meas. Sci. Technol. 9 (12) (1998) 1974–1981.
[23] K. Sangston, J. Little, M.E. Lyall, R. Sondergaard, Endwall loss reduction of high lift low pressure turbine airfils usinng profile contouring-Part II: validation, J. Tuyrbo Mach. 134 (2014) 1–10.
[24] T.G. Beckwith, R.D. Marangoni, J.H. Lienhard. Mechanical Measurements, sixth ed, Pearson Prentice Hall, New Jersey, 2007, pp. 42–45, 54-59.
[25] R.J. Moffat, Descibing the uncertainty in experimental results, Exp. Therm. Fluid Sci. 1 (3) (1988) 3–7.
[26] S.J. Kline, F.A. McClintock, Describing uncertainties in single sample experiments, ASME J. Mech. Eng. 75 (1953) 3–8.
[27] D.L. Gee, R.L. Webb, Forced convection heat transfer in helical ribbed tubes, Int. J. Heat. Mass Transf. 23 (8) (1980) 1127–1136.
[28] R.K. Shah, A.L. London, Laminar Flow Forced Convection in Ducts, Academic, New York, 1978.
[29] W.M. Kays, M.E. Crawford, Convect. Heat. Mass Transf. (1980).
[30] Kays, W.M. and London, A.L.. (1964). Compact Heat Exchangers, (2nd Edn.), McGraw-Hill, New York (1964). Meschia et al., 1967.
[31] S.A. Aasa, A.S. Shote, S.O. Giwa, M. Sharifpur, Convective thermohydraulic heat transfer enhancement of mixed dimpled geometries in rectangular channel, Elsevier J. Fuel Commun. (2021), https://doi.org/10.1016/j.jfueco.2021.100044m.